applied sciences

MDPI

Article

Tool Wear Prediction in Glass Fiber Reinforced Polymer Small-Hole Drilling Based on an Improved Circle Chaotic Mapping Grey Wolf Algorithm for BP Neural Network

Shanshan Hu [1], Hui Liu [1], Yufei Feng [1], Chang Cui [1], Yujie Ma [1,*], Genge Zhang [2,*] and Xuechuang Huang [1]

[1] College of Mechanical Engineering, Guangxi University, Nanning 530004, China
[2] Faculty of Intelligent Manufacturing, Nanning University, Nanning 530200, China
* Correspondence: mayujie_gxu@163.com (Y.M.); zhanggeng2018@sina.com (G.Z.)

Abstract: Glass fiber reinforced polymer (GFRP) is a typical difficult-to-process material. Its drilling quality is directly affected by the processing technology and tool life; burrs, tearing, delamination and other defects will reduce the service life of GFRP structural parts. Through drilling damage and tool wear experiments of GFRP, the thrust force, vibration amplitude, the number of processed holes, feed rate and cutting speed were found to be the main factors in drilling damage and tool wear. Using those main factors as the input layer, a tool wear and delamination factors prediction model was established based on an improved circle chaotic mapping (CCM) Grey Wolf algorithm for a back propagation (BP) neural network. Compared with the original BP neural network, the maximum prediction error of the improved BP neural network model was reduced by 71.2% and the root mean square (RMS) prediction error was reduced by 63.82%. The maximum prediction error of the delamination factor at the entrance was less than 3%, and the maximum prediction error of the delamination factor at the exit was less than 1%. The prediction results showed that the BP neural network model optimized by an improved circle chaotic mapping Grey Wolf algorithm can better predict the GFRP drilling quality and tool wear, and had higher accuracy, optimization efficiency and better robustness than the ordinary BP neural network.

Keywords: tool wear and prediction; glass fiber reinforced polymer (GRFP) drilling; improved Grey Wolf algorithm; BP neural network

check for updates

Citation: Hu, S.; Liu, H.; Feng, Y.; Cui, C.; Ma, Y.; Zhang, G.; Huang, X. Tool Wear Prediction in Glass Fiber Reinforced Polymer Small-Hole Drilling Based on an Improved Circle Chaotic Mapping Grey Wolf Algorithm for BP Neural Network. *Appl. Sci.* **2023**, *13*, 2811. https://doi.org/10.3390/app13052811

Academic Editors: Alessandra Caggiano and Luigi Nele

Received: 25 January 2023
Revised: 19 February 2023
Accepted: 20 February 2023
Published: 22 February 2023

Copyright: © 2023 by the authors. Licensee MDPI, Basel, Switzerland. This article is an open access article distributed under the terms and conditions of the Creative Commons Attribution (CC BY) license (https://creativecommons.org/licenses/by/4.0/).

1. Introduction

Glass fiber reinforced polymer (GFRP) is a typical difficult-to-process material. Due to the heterogeneity and anisotropy of the internal fiber, burrs, tears, delamination, and other defects often appear during drilling. Such drilling defects seriously affect the bearing capacity of the connection area, reduce the service life of the structural parts, and lead to irreversible losses in serious cases. Therefore, improving the drilling quality of GFRP and reducing processing defects are key issues to expand its applicability in industry [1,2].

In order to improve the drilling quality, much research has been carried out on the damage formation mechanism, including the proposal of a critical thrust force [3,4], the influence of the chisel edge on the critical thrust force [5], the influence of the drilling process parameters on layering [6,7], and the role of the thrust force at the outlet [8], etc. The thrust force was the main cause of hole damage, and the key to improve the quality of holes was to reduce the thrust force at the outlet. At the same time, fiber orientation [9] was also one of the main factors inducing small hole damage.

Faced with many defects in GFRP hole processing, an effective way to improve the small-hole quality is by improving the tool materials and structures. Studies included the impact of the tool coating [10], tool materials [11], tip shape [12], drill bit number [13] and tool geometric angle [14] on small hole damage and tool wear.

In recent years, some scholars have tried to use intelligent algorithms to establish the relationship between the hole quality and its influencing factors, so as to identify, judge and predict the drilling quality. In 2009, R Mishra [15] set up a three-layer artificial neural network (ANN) to predict the drilling-induced damage of GFRP by using the drill point geometry, spindle speed, feed rate and drill diameter as the input layer, and the ratio of the damage area to the hole area as the output layer. This was an early attempt to use intelligent algorithms to predict GFRP drilling characteristics, while an adaptive learning rate was chosen and the rate of convergence was reduced to make the results more reliable. Rasmi Ranjan Behera [16] used an ANN algorithm to simultaneously predict the delamination and surface roughness of the GFRP drilling process. This is the first application of a neural network to simultaneously predict the delamination and surface roughness of the GFRP, and used a trial and error method to determine the 'right number' of hidden layer neurons.

Azmi [17] established the first tool wear prediction model for end milling of GFRP composites through fuzzy logic modelling combined with neural network training and found that the ANFIS model applied to the same dataset was effective in reducing the error in predicting tool wear during end milling of composites. Sathish Rao U15 [18] constructed an ANN network to predict flank wear of an HSS drill bit during drilling of GFRP composite laminates by using spindle speed, drill feed and drill diameter and selected the optimal network structure for predicting the flank wear of a drill bit by comparing the mean square error values from seven different artificial neural network back propagation algorithms. Although the selected supervised algorithm was the fastest, it required more memory compared to the other algorithms. However, the reasons for choosing model input layer parameters are not given in detail. At the same time, there are a number of factors that influence the quality of GFRP small hole drilling processes, which play a dominant role in the prediction of process quality, but have not been discussed. Therefore, it is worth exploring how the model can be optimised to better extract features.

Many scholars have used algorithm-optimized ANNs to establish machining quality prediction models, which effectively improves the prediction accuracy. Ahmed Belaadi [19] evaluated the effect of drill diameter, feed rate and spindle speed on the drilling process of jute/polyester biocomposites with the desirability/RSM and ANN/genetic algorithm (GA) curve. The results of the study showed that the correlation of the ANN coefficients was higher than the RSM coefficients and the model was more accurate. Shashi Prakash [20] used artificial neural networks to predict the depth and surface roughness of GFRP after CO_2 laser milling and found that the milling depth predicted using this ANN model outperformed the results of the semiempirical model. Huajun Cao [21] developed a prediction model for the milling surface quality of unidirectional carbon fiber/poly-ether-ether-ketone laminates by using a genetic-algorithm-optimized back propagation (GA-BP) neural network. Prakhar Kumar Kharwar [22] predicted the average surface roughness, cutting force and material removal rate during end milling of multiwall carbon nanotube/epoxy nanocomposites using a grey relational analysis and Grey Wolf optimization (GRA-GWO) algorithm, which showed that GRA-GWO had a higher convergence rate and effectively improved the required machining performance. The above literature provides valuable insights on how to assess and predict GFRP drilling quality.

This paper discussed the factors that influence tool wear and drilling quality by conducting drilling damage and tool wear experiments of GFRP. Based on an improved circle chaotic mapping Grey Wolf algorithm for a BP neural network, a prediction model of the tool wear and delamination factors was established. It can provide a method to estimate the small-hole quality and monitor on-line the tool wear during GFRP drilling.

2. Experiments

2.1. Workpieces and Drill Bits

The GFRP (FR-4, Shenzhen XiongYihua Plastic Materials Co., Ltd., Shenzhen, China) is produced by high-temperature moulding, in which the high-strength glass fiber cloth is the matrix and epoxy resin is the reinforcement. Its size is 80 mm × 80 mm × 6 mm, as shown in Figure 1a, the fiber fraction is 60%, and 20 layers of fiber are laid as [0°/90°].

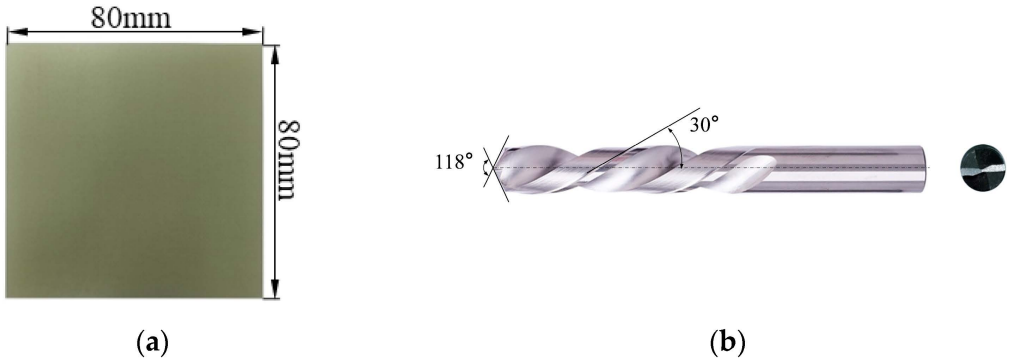

Figure 1. Physical map of workpiece and drill bit. (**a**) Workpiece; (**b**) The integral carbide drill bit.

The integral carbide drill bit (YG6, Zhuzhou Cemented Carbide Group Co., Ltd., Zhuzhou, China) with a diameter of 6 mm is used. The point angle is 118°, and helix angle is 30°, as shown in Figure 1b. Its hardness is 89.5 MPa, bending strength is 1450 MPa, and impact toughness is 2.6 J/cm.

2.2. Experimental Platform

Figure 2 is the experiment platform. The experiment was carried out on a FANUC ROBODRILL_a-T14iFLb vertical machining centre with a maximum spindle speed of 24,000 r/min. The thrust force signal was collected by a Kistler 9257B piezoelectric dynamometer (Kistler Group, Inc., Winterthur, Switzerland) and a Kistler 5070A charge amplifier (Kistler Group, Inc., Winterthur, Switzerland). The vibration signal was collected by a PCB 356A01 triaxial sensor (PCB Piezotronics, Inc., Buffalo, NY, USA) and recorded by an NI 9234 sound and vibration module (National Instruments Corporation, Austin, TX, USA). The LabVIEW Software was used to analyse the vibration signals.

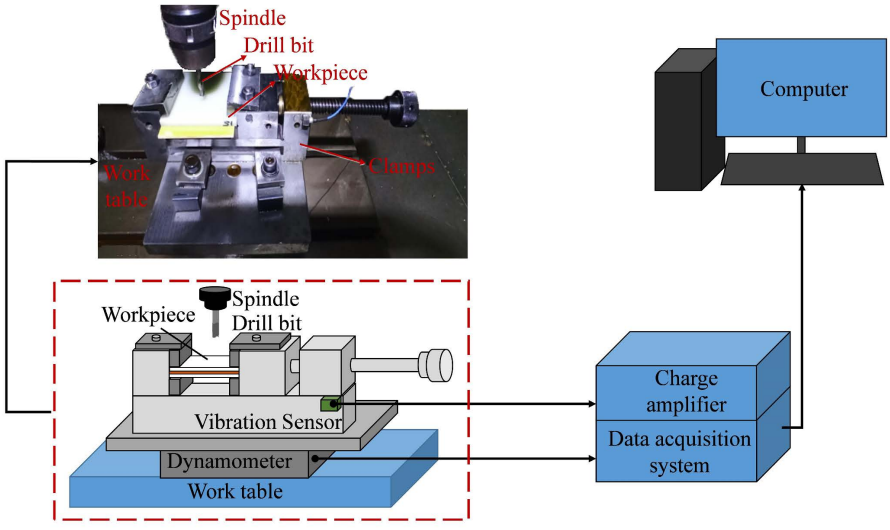

Figure 2. The experiment platform.

2.3. Morphology Observation Method and Equipment

The wear morphology was observed using a three-dimensions (3D) super depth-of-field microscope (VHX-500FE, KEYENCE, Osaka, Japan). In order to evaluate the tearing degree of the GFRP after processing, we adopted the evaluation method for hole delamination of fiber composite materials proposed by Davim and Rubio et al., namely the delamination factor method [23], as shown in Figure 3. The delamination factor F_d is defined as

$$F_d = \frac{Dmax}{D} \tag{1}$$

where $Dmax$ is the diameter of the maximum circle involving the tear zone, and D is the ideal diameter of the hole, also known as the tool diameter. F_dR is the delamination factor at the entrance, and F_dC is the delamination factor at the exit.

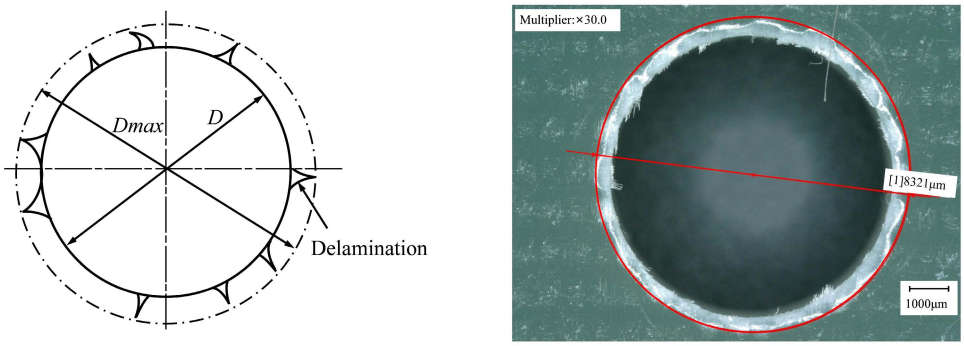

(**a**) (**b**)

Figure 3. Diagram of F_d. (**a**) Measurement diagram of F_d. (**b**) Measurement by microscope.

2.4. Experimental Scheme

After the comparison of the pre-test, this experiment used the dry drilling method without the support plate. Based on the parametric experimental investigation, three common cutting parameters were selected, namely cutting speed, feed rate [24–26] and tool diameter [27,28]. In order to ensure the rationality of processing parameters, several pre-experiments were carried out with different cutting parameters according to reference [29]. The single factor experimental scheme of the influence of the cutting parameters on the thrust force and vibration is shown in Table 1. Each experimental set was repeated three times to obtain the average value.

Table 1. Single factor experimental scheme of the influence of the cutting parameters on the thrust force and vibration.

Drilling Parameters	Value
Cutting speed V_c (m/min)	25, 45, 65, 85, 105
Feed rate f (mm/min)	10, 30, 50, 70, 90
Drill bit diameter (mm)	6, 8, 10

The number of holes and the wear width of the flank face (VB) were taken as performance indexes. The single factor experimental scheme of the tool wear is shown in Table 2. We used a new drill bit at the beginning of each experiment, and measured the VB by the 3D super depth-of-field microscope for drilling every 25 holes.

Table 2. Single factor experimental scheme of tool wear.

Cutting Speed V_c (m/min)	Feed Rate f (mm/min)	Number of Drilling Holes
45	30	25, 50, 75, 100, 125, 150, 175, 200
65	30	25, 50, 75, 100, 125, 150, 175, 200
85	30	25, 50, 75, 100, 125, 150, 175, 200
85	50	25, 50, 75, 100, 125, 150, 175, 200
85	70	25, 50, 75, 100, 125, 150, 175, 200

3. Results and Discussion

3.1. Factors Influencing the Entrance and Exit Delamination Factors

3.1.1. Influence of Cutting Speed on the Entrance and Exit Delamination Factors

Figure 4 shows the morphology of the entrance and exit at different cutting speeds, and Figure 5 shows the entrance and exit delamination factors at different cutting speeds. According to Figure 5b,c, the delamination factors of the entrance and exit gradually decreased with the increase of cutting speed. However, the delamination factor of the exit was significantly greater than that of the entrance. This may be due to the pushing action of the chisel edge of the drill bit at the exit, which made the stripping of the fiber more serious, and the delamination factor of the exit was larger. According to reference [3–5], the main cause of delamination on the pore surface was the thrust force in the drilling process. From Figures 4 and 5, the greater the cutting speed, the smaller the thrust force, and the lower the entrance and exit delamination factors. In addition, the large amount of cutting heat generated in the drilling process raised the drilling temperature and melted the resin matrix, which had a significant impact on the delamination tearing at the hole exit [1].

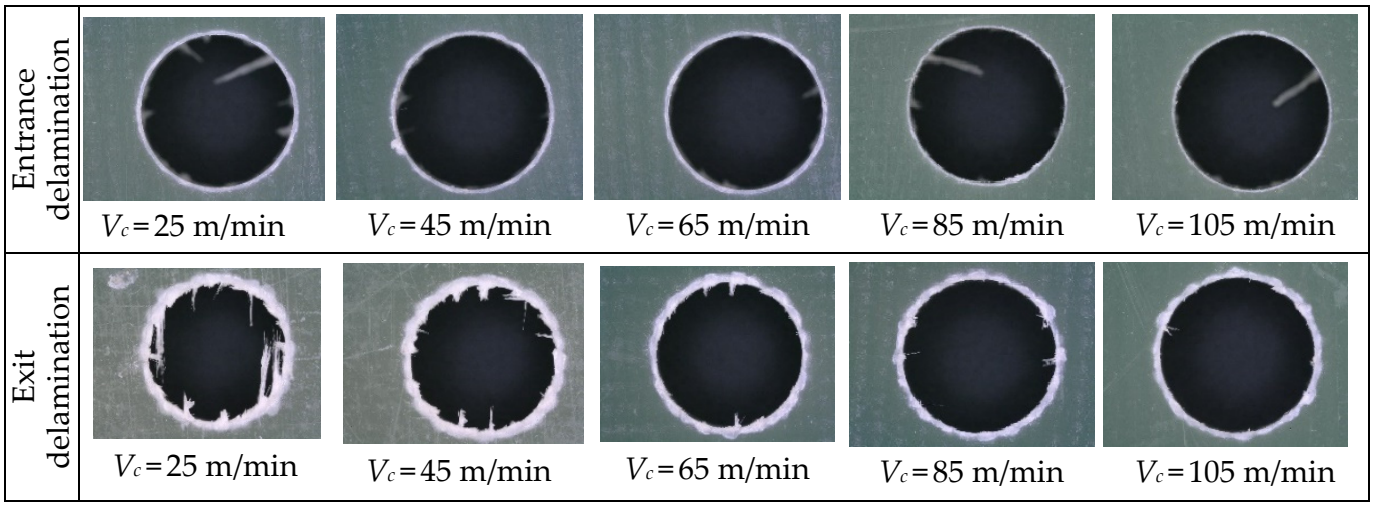

Figure 4. Morphology of entrance and exit at different cutting speeds (f = 10 mm/min, drill bit diameter = 6 mm).

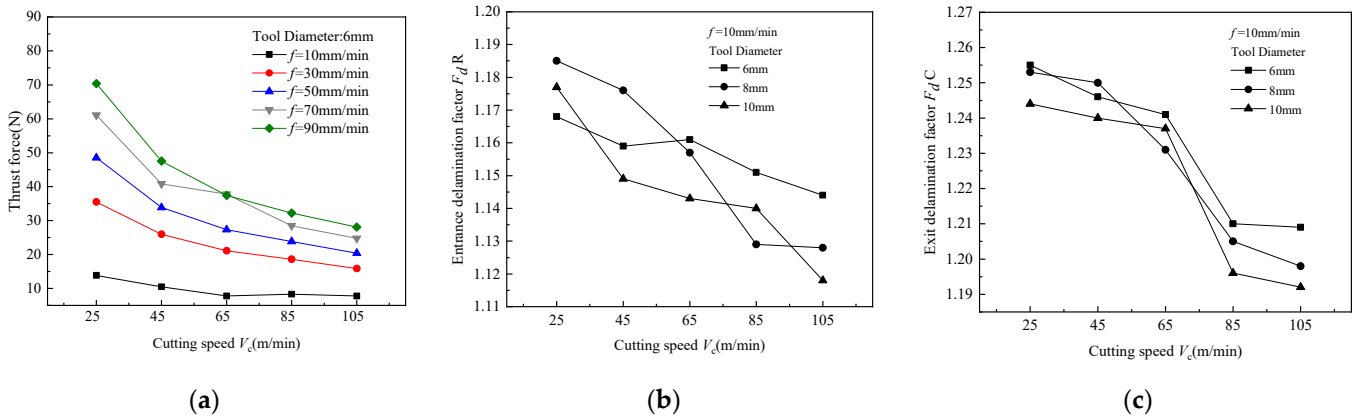

(**a**) (**b**) (**c**)

Figure 5. Entrance and exit delamination factors at different cutting speeds. (**a**) Effect of cutting speed on thrust force at different feed rates; (**b**) Entrance delamination factors at different cutting speeds; (**c**) Exit delamination factors at different cutting speeds.

3.1.2. Influence of Feed Rate on the Entrance and Exit Delamination Factors

Figure 6 shows the morphology of the entrance and exit at different feed rates, and Figure 6 shows the entrance and exit delamination factors at different feed rates. With the increasing feed rate, the thrust force increased gradually, and the delamination factor of the entrance and exit also increased, as shown in Figure 7. At the entrance, with the increase of the feed rate, the pushing force of the chisel edge was greater than the shearing force, and part of the fiber was torn apart. At the exit, as the feed rate increased, the drill bit moved quickly across the workpiece, and the cutting edge did not have enough time to cut through the internal glass fibers. Therefore, a large number of fibers were torn apart and pulled out of the resin.

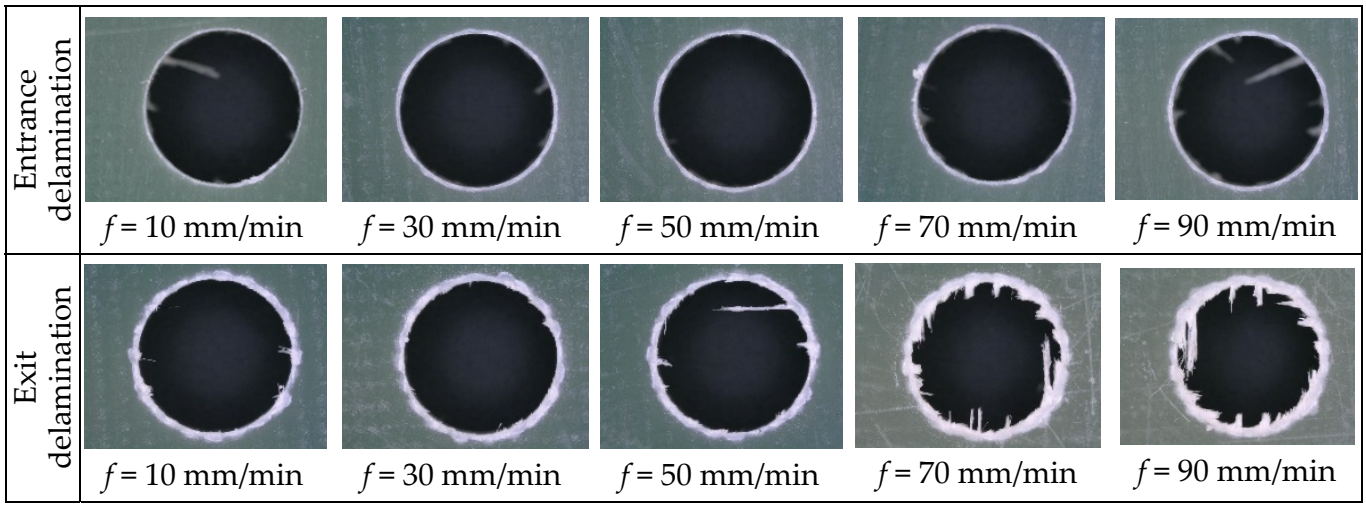

Figure 6. Morphology of entrance and exit at different feed rates (V_c = 85 m/min).

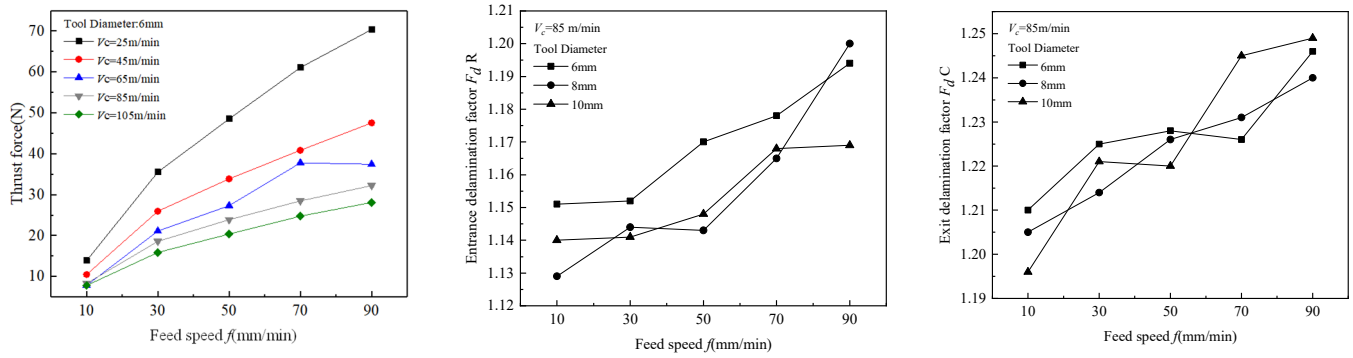

(**a**) (**b**) (**c**)

Figure 7. Entrance and exit delamination factors at different feed rates. (**a**) Effect of feed rate on thrust force at different cutting speeds. (**b**) Entrance delamination factors at different feed rates. (**c**) Exit delamination factors at different feed rates.

Obviously, the delamination factor was directly related to the feed rate and cutting speed.

3.2. Factors Influencing the Tool Wear

3.2.1. Wear Morphologies of Different Parts of the Drill Bit

Figure 8 shows the wear morphologies of different parts of the drill bit.

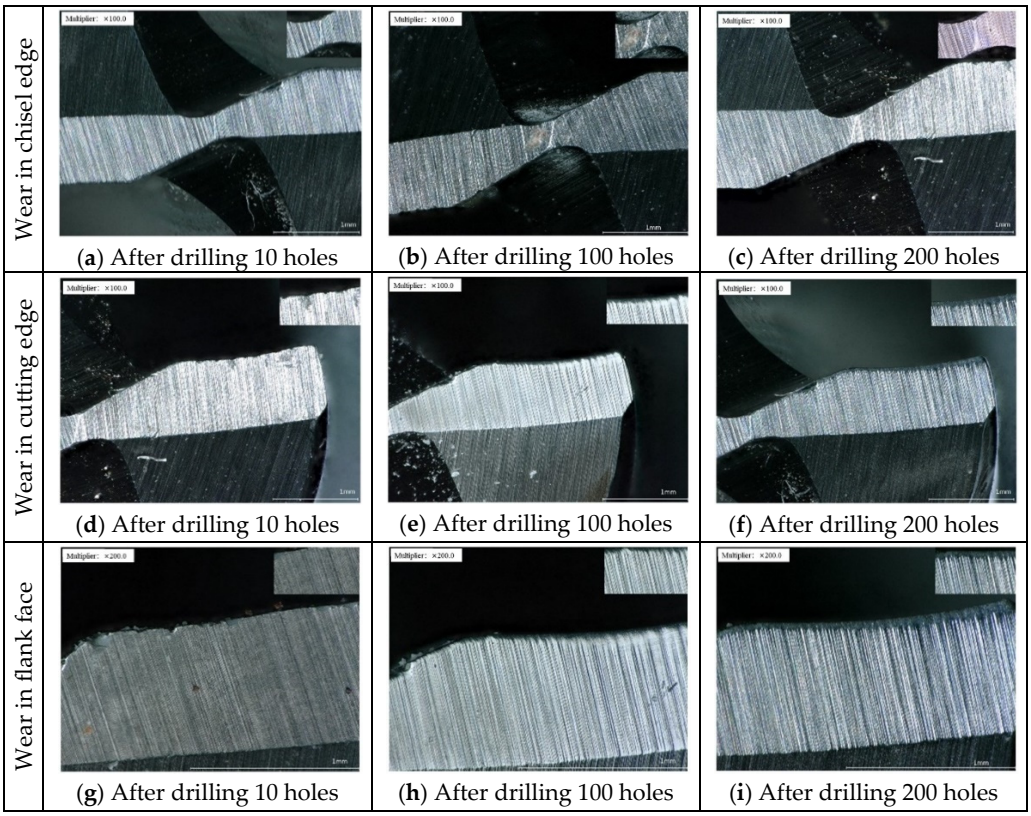

Figure 8. Wear morphologies of different parts of the drill bit (Vc = 85 m/min, f = 30 mm/min).

Figure 8a–c shows the wear in the chisel edge. When the drilling process began, first the chisel edge came into contact with the material, but its linear velocity was the lowest. Plastic deformation occurred under the extrusion of the chisel edge. As the machining length increased, the chisel edge was offset in the radial and tangential directions.

Figure 8d–f shows the wear in the cutting edge. With the increase of the machining length, the cutting edge gradually changed from a straight line to a concave arc. This indicated that different parts of the cutting edge were subjected to different loads. The middle of the cutting edge was the main cutting part and the main channel of chip outflow. It suffered the greatest contact stress, so it wore the most.

Figure 8g–i shows the wear in the flank face. Due to continuous friction with the glass fiber and resin matrix in the machining area, the flank face wear was significant, and the expansion of the tool wear zone increased the contact area with the material, which further exacerbated the wear. With the increase of machining time, a wear band of different widths was formed on the flank face. It was narrower near the centre of the drill bit and wider near the outer corner.

According to the wear patterns of the different parts of the drill bit, VB can be selected as the performance index to evaluate the wear.

3.2.2. Influence of Drilling Parameters on the Tool Wear

Figure 9 is the VB value at different drilling parameters. When the feed rate was the same, the higher the cutting speed, the longer the machining distance of the cutting edge in unit time, and the more severe the tool wear, as seen in Figure 9a. At the cutting speed of 85 m/min, machining about 100 holes was the dividing point of the severe wear stage, and the VB of the drill bit rose rapidly.

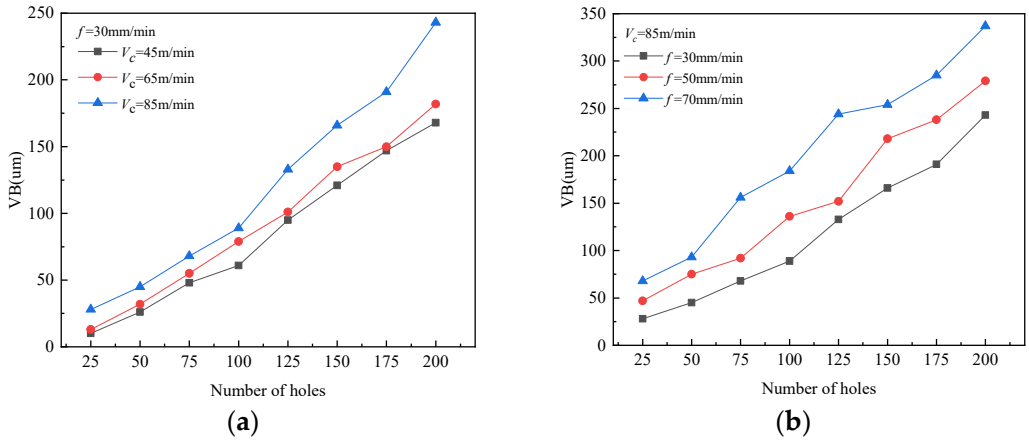

Figure 9. VB at different drilling parameters: (**a**) different cutting speeds; (**b**) different feed rates.

When the cutting speed was the same, the higher the feed rate, the greater the material removal rate of every cutting edge, and the more severe the tool wear, as shown in Figure 9b. When 200 holes were drilled, VB was 243 μm at the low feed rate of 30 mm/min; at the high feed rate of 70 mm/min, VB reached 337 μm. When the feed rate was higher than 70 mm/min, the drill bit needed to be sharpened or changed to ensure the machining quality and the stability of the drilling system.

Therefore, the feed rate, cutting speed and the number of holes were the main factors influencing the tool wear and should be considered as the input data of the prediction model.

3.3. Effect of Tool Wear on Drilling Dynamic Characteristics

Figure 10 shows the effect on the thrust force of tool wear under different drilling parameters. As seen in Figure 10a, with the increase of the number of holes, the thrust force remained high but increased slowly at low cutting speed. At the higher cutting speeds of 65 and 85 m/min, the thrust force increased rapidly. Especially, the thrust force increased by 34.8% when Vc = 85 m/min. At low feed rate, the thrust force was low and tool wear had no significant effect on it. However, it increased significantly with the increase of the feed rate. When f = 70 mm/min, the thrust force increased by 47.9%.

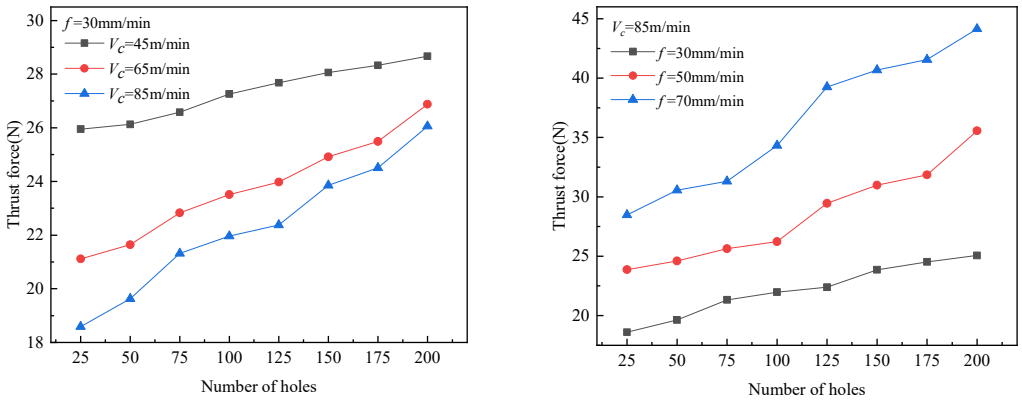

Figure 10. Effect of tool wear on the thrust force: (**a**) different cutting speeds; (**b**) different feed rates.

As shown in Figure 11, the influence of tool wear on the vibration amplitude under different drilling parameters was similar to that on the thrust force. At the high cutting speed of 85 m/min, the vibration amplitude increased by 53.6%; and at the high feed rate of 70 mm/min, it increased sharply by 68.9%. Studies [30] showed that wear rate was a function of force and velocity. Therefore, the thrust force and vibration amplitude reflected the tool wear state in an agile way. They can be selected as the input data for predicting the tool wear and delamination factors.

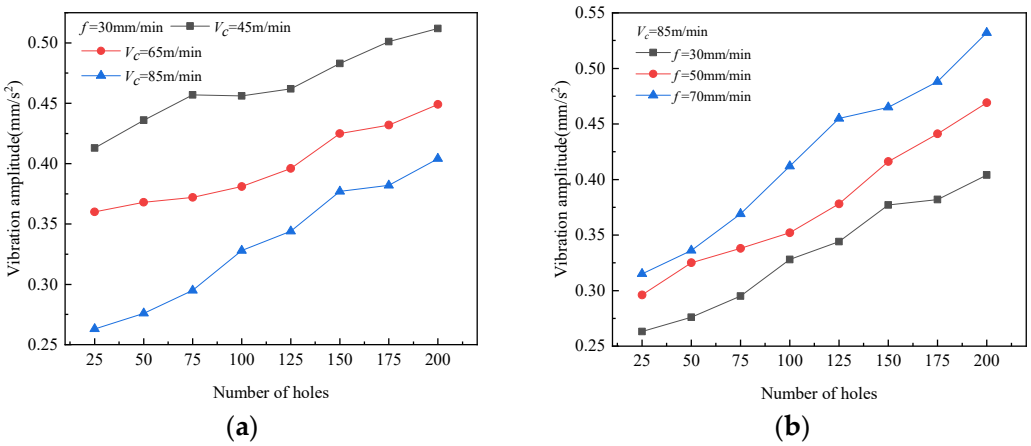

Figure 11. Effect of tool wear on the vibration amplitude: (**a**) different cutting speeds; (**b**) different feed rates.

3.4. Effect of Tool Wear on the Entrance and Exit Delamination Factors

Figure 12 shows the effect of tool wear on the delamination factors. With the increase of the number of holes, the delamination factors both showed a trend of increasing, but the growth rate of the exit delamination factors was significantly higher than that of the entrance delamination factors. Because the worn tool cannot cut the material sufficiently, fibers were increasingly torn at the edges of the holes. Therefore, the value of the delamination factors at the entrance and exit reflected the change of the VB. Combined with Figures 10 and 12, when the feed rate was as low as 30 mm/min, the variation trend of the delamination factors was basically the same as that of the thrust force; however, when the feed rate was as high as 70 mm/min, the thrust force increased less than the delamination factors. Therefore, both of them should be used as the main influencing factors to predict tool wear.

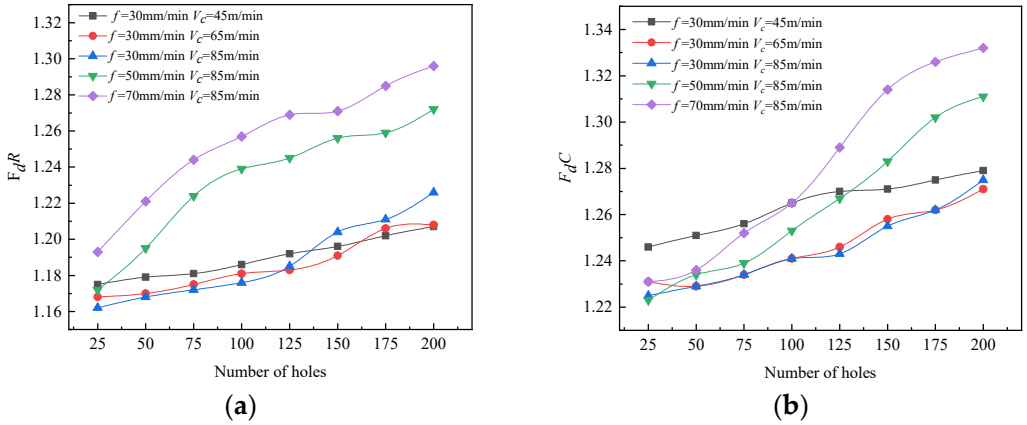

Figure 12. Effect of tool wear on the delamination factors: (**a**) entrance delamination factors; (**b**) exit delamination factors.

According to the wear mechanism diagram established by Sathish Rao Udupi [31], the wear rate gradually increased with increasing spindle speed and feed rate. It was found that the increase in spindle speed and feed rate within the different stages of wear not only led to changes in the tool wear mechanism, but also had a huge impact on the surface quality and delamination factors. Furthermore, the increase in tool wear was not only related to the machining conditions, but also depended on the forces generated during machining [17]. Combining the results of the analysis in Figures 9 and 11, the delamination factor with the axial force should be selected as the input layer of the neural network for the prediction of tool wear.

4. The Tool Wear Prediction Model Based on an Improved Circle Chaos Mapping Grey Wolf Algorithm for BP Neural Network

4.1. BP Neural Network Structure Based on Improved Grey Wolf Algorithm

4.1.1. BP Neural Network

Artificial Neural Network (ANN) is a mathematical model that is closer to the properties of biological neural networks than any other machine learning algorithm. By simulating the structure and function of a biological neural network, an ANN consists of a large number of interconnected neurons that can be used to establish complex relationships between data models. A commonly used artificial neural network is the BP neural network, which consists of the input layers, hidden layers and output layers [32,33]. Each layer has its own neural network connected to the next layer. The input layer is mainly used to obtain input information. The hidden layer mainly carries out "feature extraction", adjusting the weight to make the neural units of the hidden layer respond to certain patterns. The output layer is used to interconnect with the hidden layer and output model results. The weight is adjusted to form the correct response to different hidden layer neuron stimulation.

4.1.2. Grey Wolf Algorithm

The Grey Wolf Optimiser [34] is a swarm intelligence optimisation algorithm inspired by grey wolves, which mimics the social hierarchy and hunting behaviour of grey wolves. It divides the grey wolf into four leadership classes—alpha, beta, delta, and omega, and divides hunting behaviour into three steps—seeking prey, encircling prey, and attacking prey. In the Grey Wolf algorithm, the optimal solution is considered to be alpha, the second and third best solutions are named beta and delta, and omega is the remaining alternative. To mathematically model the encircling behaviour of the grey wolf during hunting, the following equations are proposed [34]:

$$\vec{D} = \mid \vec{C} \cdot \vec{X}_p(t) - \vec{X}(t) \mid \tag{2}$$

$$\vec{X}(t+1) = \vec{X}_p(t) - \vec{A} \cdot \vec{D} \tag{3}$$

where t indicates the current iteration, $\vec{D}$ is the distance between wolf and prey, $\vec{A}$ and $\vec{C}$ are coefficient vectors, $\vec{X}_p$ is the position vector of the prey, and $\vec{X}$ Indicates the position vector of a grey wolf. The vectors $\vec{A}$ and $\vec{C}$ are calculated as follows:

$$\vec{A} = 2\vec{a} \cdot \vec{r}_1 - \vec{a} \tag{4}$$

$$\vec{C} = 2 \cdot \vec{r}_2 \tag{5}$$

where components of $\vec{a}$ are linearly decreased from 2 to 0 over the course of iterations and r_1, r_2 are random vectors in [0, 1].

It is known that the Grey Wolf algorithm has a strong local search ability, but the population difference is small and it is easy for it to fall into the local solution. In the face of complex problems, its global search ability is poor. Therefore, it is necessary to optimize the initial population of the Grey Wolf algorithm.

4.1.3. The Initial Population Optimized by Circle Chaotic Mapping (CCM)

The CCM is defined as

$$x_{i+1} = mod(x_i + 0.2 - (\frac{0.5}{2\pi}) \sin(2\pi x_i), 1) \tag{6}$$

CCM is used to replace iterative Equations (2) and (3) [34] to change the initial population of grey wolves. Compared with the randomly distributed population, the initial position distribution of the improved one is more uniform. In this way, the search scope of the grey wolf is expanded, and the defect that the algorithm falls easily into a local solution is improved to a certain extent. The optimization efficiency of the algorithm is improved.

4.1.4. A Neural Network Improved by Grey Wolf Algorithm Based on Circle Chaotic Mapping

In this paper, an improved CCM Grey Wolf algorithm for a BP neural network and a BP neural network without improvement were compared by predicting the tool wear and the delamination factors. Figure 13 shows the flow chart of the BP neural network improved by the Grey Wolf algorithm based on CCM. According to the analysis in Sections 3.1–3.4 above, the cutting speed, feed rate, number of processed holes, thrust force and vibration amplitude have significant effects on the tool wear and delamination factors. These factors are selected as the input layer of the neural network. The output layer comprises the VB of tool wear and the entrance and exit delamination factors. The diagram of the BP neural network structure is shown in Figure 14.

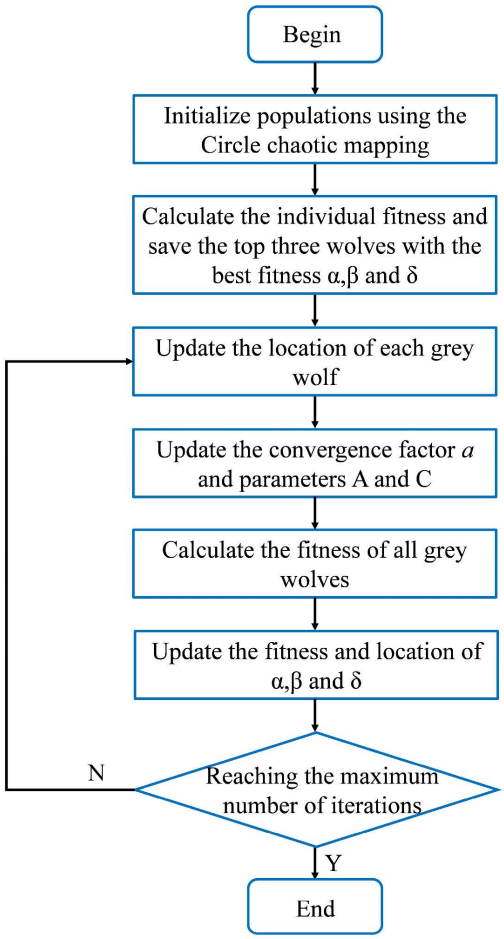

Figure 13. Flow diagram of the improved neural network structure [34].

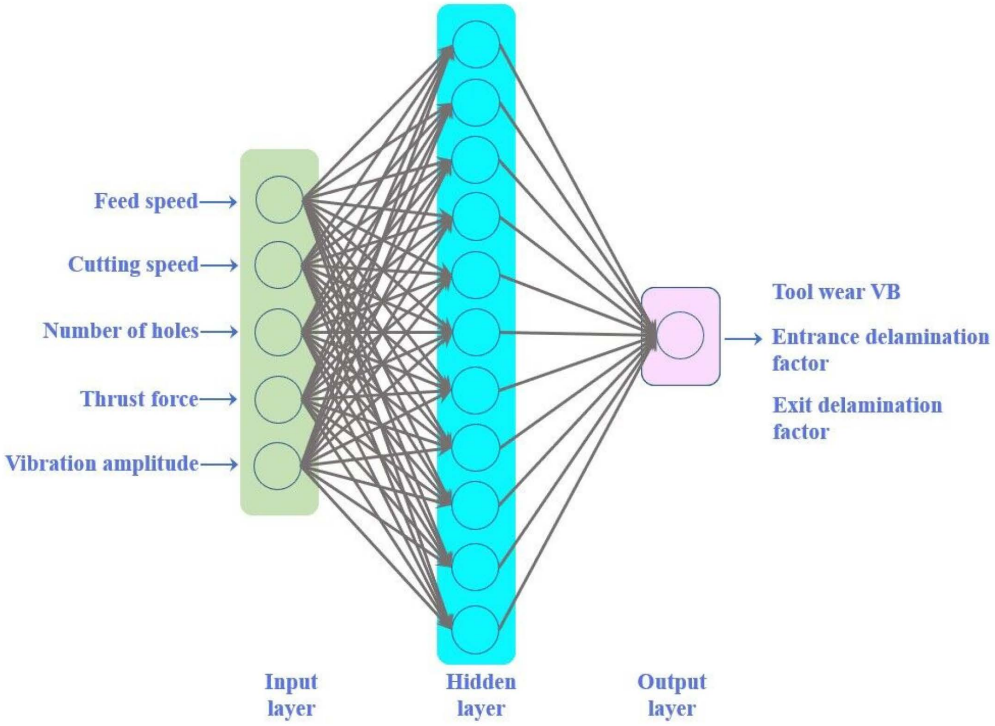

Figure 14. BP neural network prediction model.

According to empirical Formula (3), the number of hidden layer neurons m is determined as follows:

$$m = \sqrt{n + l} + \alpha \quad (7)$$

where n is the number of input layer neurons, and l is the number of output neurons. α is a constant between 1 and 10. According to Figure 13, when α = 8, the number of hidden layer neurons m is 11. The transfer function between the layers is the tan-sigmoid function.

4.2. Model Training

Using the method shown in Figure 13, each initial weight was optimized by the CCM, then a random value was generated within [−1, 1]. The learning rate of the neural network model is set as 0.01, the maximum number of training times as 1000, and the expected error as 0.0001. After the network parameters were determined, the experimental results were used to train the model. Table 3 shows the training data of the network model. Using the holdout test, the original sample set was randomly divided into 32 sets of data as the training set and 8 sets of data as the prediction set.

Table 3. Training data for the neural network.

Feed Rate f (mm/min)	Cutting Speed V_c (m/min)	Number of Holes	Thrust Force F_z (N)	Vibration Amplitude P_z (mm/s^2)	VB (um)	F_dR	F_dC
30	45	25	25.95	0.413	10	1.175	1.246
		50	26.13	0.436	26	1.179	1.251
		75	26.58	0.457	48	1.181	1.256
		100	27.26	0.456	61	1.186	1.265
		125	27.68	0.462	95	1.192	1.263
		150	28.06	0.483	121	1.196	1.271
		175	28.33	0.501	147	1.202	1.275
		200	28.67	0.512	168	1.207	1.279
30	65	25	21.11	0.36	13	1.168	1.231
		50	21.64	0.368	32	1.17	1.229
		75	22.83	0.372	55	1.175	1.234
		100	23.51	0.381	79	1.181	1.241
		125	24.68	0.396	101	1.183	1.246
		150	24.92	0.425	135	1.191	1.258
		175	25.49	0.432	150	1.206	1.262
		200	26.88	0.449	182	1.208	1.271
30	85	25	18.59	0.263	28	1.162	1.225
		50	19.63	0.276	45	1.168	1.229
		75	21.32	0.295	68	1.172	1.234
		100	21.96	0.328	89	1.176	1.241
		125	22.38	0.344	133	1.185	1.243
		150	23.86	0.377	166	1.204	1.255
		175	24.51	0.382	191	1.211	1.262
		200	25.06	0.404	243	1.226	1.275

Table 3. *Cont.*

Feed Rate f (mm/min)	Cutting Speed V_c (m/min)	Number of Holes	Thrust Force F_z (N)	Vibration Amplitude P_z (mm/s^2)	VB (um)	F_dR	F_dC
50	85	25	23.87	0.296	47	1.172	1.223
		50	24.59	0.325	75	1.195	1.234
		75	25.63	0.338	92	1.224	1.239
		100	26.22	0.352	136	1.239	1.253
		125	27.45	0.378	152	1.245	1.267
		150	27.98	0.416	218	1.256	1.283
		175	28.85	0.441	238	1.259	1.302
		200	30.56	0.469	279	1.272	1.311
70	85	25	28.48	0.315	68	1.193	1.231
		50	30.56	0.336	93	1.221	1.236
		75	31.91	0.369	156	1.244	1.252
		100	33.32	0.412	184	1.257	1.265
		125	35.26	0.455	244	1.269	1.289
		150	37.68	0.465	254	1.271	1.314
		175	41.56	0.488	285	1.285	1.326
		200	42.14	0.532	337	1.281	1.332

MATLAB software (version: R2020b) was used to train the neural network. The training results are shown in Figure 15. The training results showed that the error was small and the training was effective.

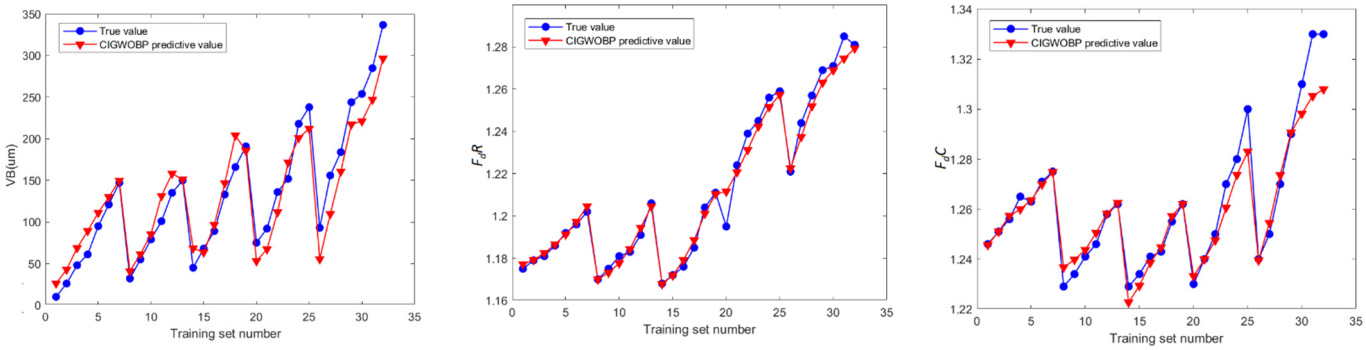

(**a**) (**b**) (**c**)

Figure 15. Training results: (**a**) VB; (**b**) F_dR; (**c**) F_dC.

4.3. Model Prediction

Eight groups of test data in Table 3 were used for prediction. The comparison of the true value, the unimproved BP neural network predicted value and the improved BP neural network predicted value is shown in Figure 16.

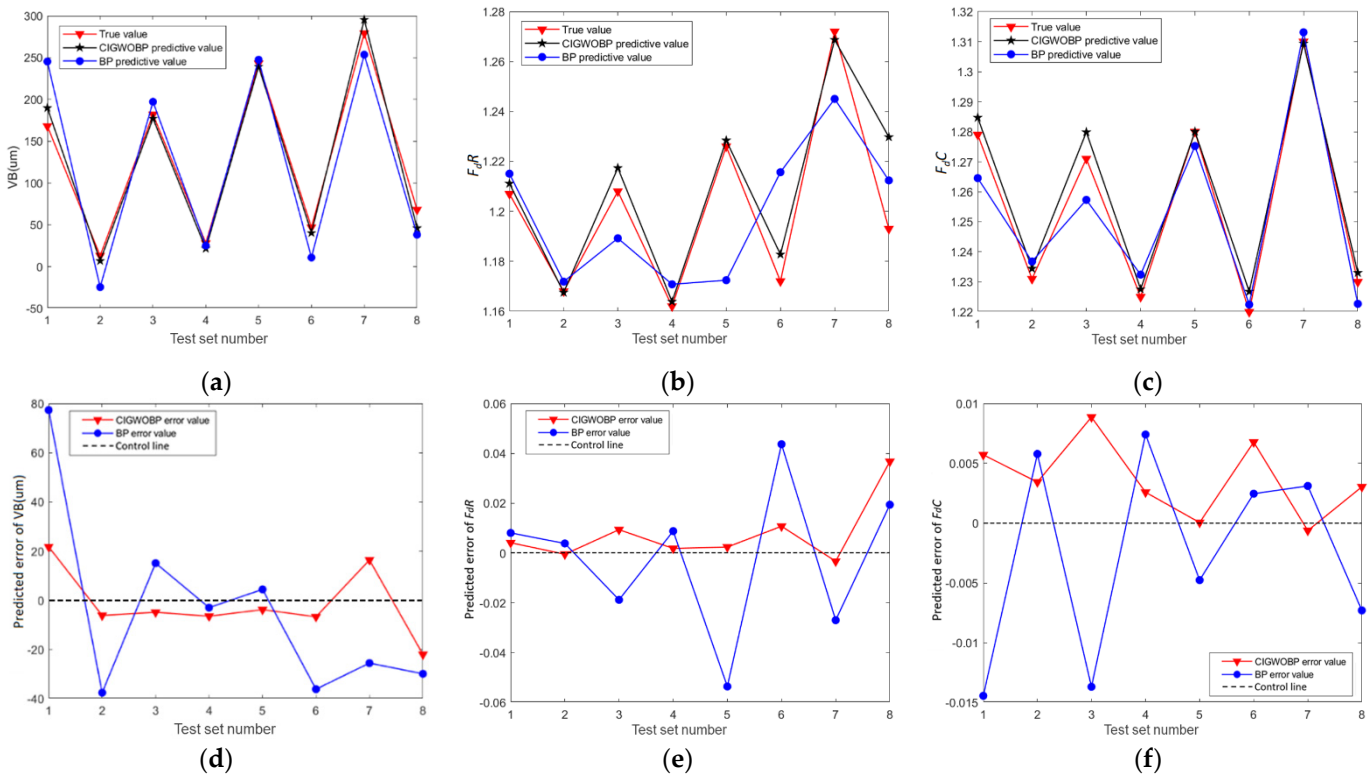

Figure 16. Prediction results: (**a**)VB; (**b**) F_dR; (**c**) F_dC; (**d**) error of VB; (**e**) error of F_dR; (**f**) error of F_dC.

The error between the predicted value and the true value of the neural network model optimized by the improved Grey Wolf algorithm was much smaller than that between the predicted value and the true value of the ordinary BP neural network. The maximum prediction error of VB optimized by the improved Grey Wolf algorithm was 22.54 μm, which was 71.2% smaller than that of the BP neural network at 78.33 μm. The root mean square (RMS) error of VB optimized by the improved Grey Wolf algorithm was 13.21 μm, which was 63.82% less than the average value of the BP neural network, and was less than 10% of the average true value. The prediction error of F_dR was not more than 3%, and the prediction error of F_dC was not more than 1%. Therefore, the neural network model optimized by the improved Grey Wolf algorithm can better predict the drilling quality of GFRP, and had higher accuracy and optimization efficiency than the ordinary BP neural network.

The scatter plot shown in Figure 17 shows the linear correlation between the predicted values of the neural network and the experimental results. The coefficient of determination (R^2) indicated the degree of fit between the experimental results and the predicted values. the R^2 of the training set for VB, F_dR and F_dC were 0.9651, 0.9793 and 0.9228, respectively, and that of the test set were 0.9898, 0.9172 and 0.9911. It indicated that the predicted values of the neural network in the training and test sets fitted well with the experimental values.

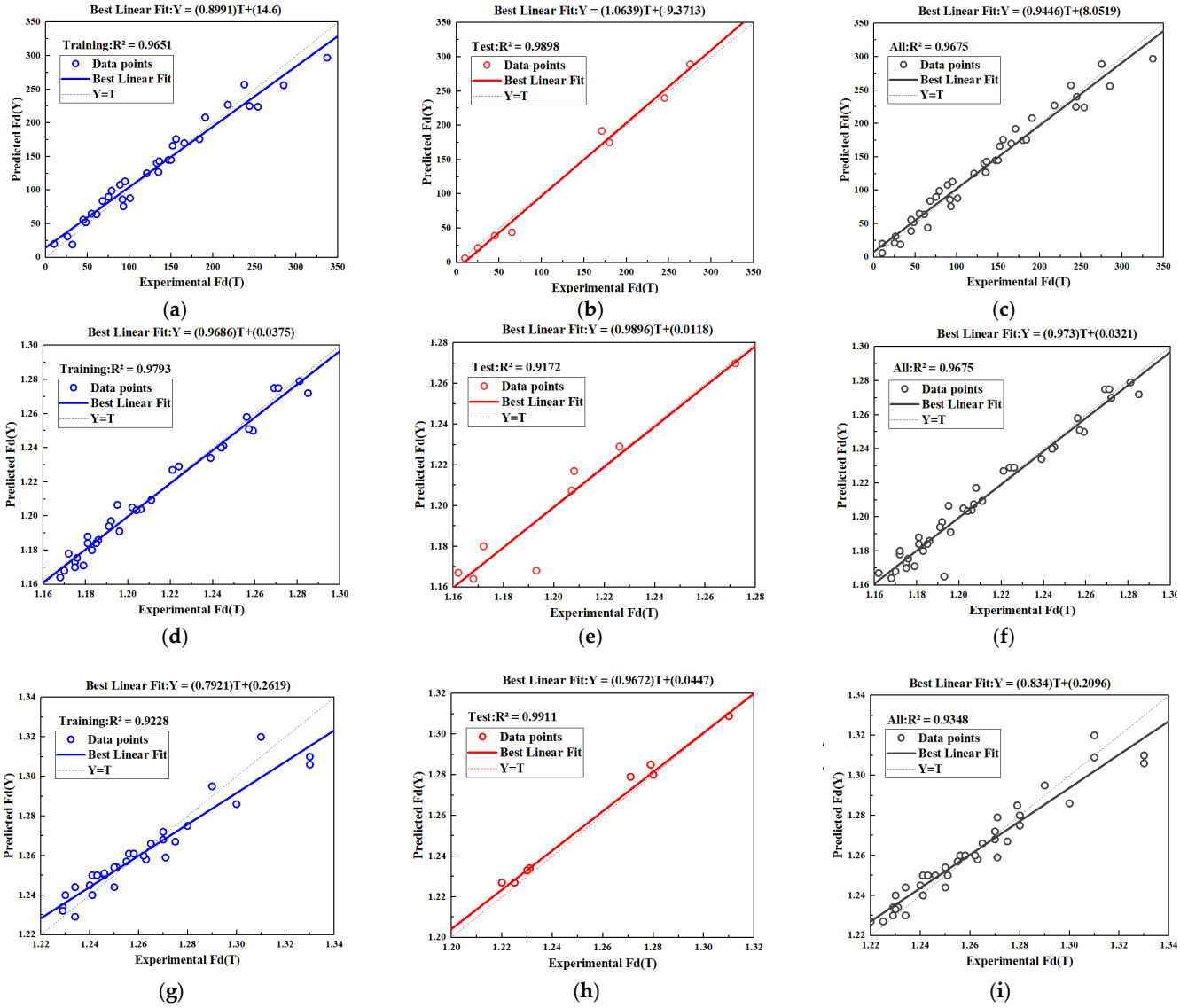

Figure 17. The correlation coefficient between predicted and experimental values. (**a**) R-value of the training set for VB. (**b**) R-value of the test set for VB. (**c**) R-value of the training set and test set for VB. (**d**) R-value of the training set for F_dR. (**e**) R-value of the test set for F_dR. (**f**) R-value of the training set and test set for F_dR. (**g**) R-value of the training set for F_dC. (**h**) R-value of the test set for F_dC. (**i**) R-value of the training set and test set for F_dC.

5. Conclusions

Aiming at the problems of drilling damage and tool wear when drilling GFRP, experiments on the characteristics of the drilling damage and tool wear of GFRP were carried out in this paper. It was found that the thrust force, vibration amplitude, the number of processed holes, feed rate and cutting speed were the main factors affecting the drilling damage and tool wear. By comprehensive consideration of the above processing dynamic characteristics and processing parameters, an improved CCM Grey Wolf algorithm for a BP neural network was developed to predict the tool wear and delamination factors. The main conclusions were as follows:

1. The higher the cutting speed, the smaller the thrust force, and the lower the entrance and exit delamination factors. With the increasing feed rate, the thrust force increased gradually, and the delamination factor of the entrance and exit also increased. The delamination factor was directly related to the feed rate and cutting speed, and these two parameters can be selected as input layers for delamination factor prediction.

2. Due to continuous friction with the glass fiber and resin matrix in the machining area, the flank face wear was significant, and the expansion of the tool wear zone increased the contact area with the material, which further exacerbated the wear. The VB of the flank face can be selected as the performance index to evaluate the wear.
3. The higher the feed rate and cutting speed, the more severe the tool wear. The feed rate, cutting speed and the number of holes were the main factors influencing the tool wear and should be used as the input data of the prediction model. Because the worn tool cannot cut the material sufficiently, fibers were increasingly torn at the edge of the entrance and exit. Therefore, the value of the delamination factors at the entrance and exit reflected the change of the value of VB.
4. A BP neural network model improved by the CCM Grey Wolf algorithm was proposed to predict the processing quality and tool wear of GFRP drilling. The maximum prediction error of the improved BP neural network model was reduced by 71.2%, and the RMS prediction error was reduced by 63.82%. The prediction error of F_dR was not more than 3%, and the prediction error of F_dC was not more than 1%. The prediction results showed that the neural network model optimized by the improved Grey Wolf algorithm can better predict the drilling quality and tool wear of GFRP, and has higher accuracy, optimization efficiency and better robustness than the ordinary BP neural network.

Author Contributions: Conceptualization, S.H., Y.F. and C.C.; methodology, S.H. and Y.M.; software, Y.F. and Y.M.; validation, S.H., H.L. and G.Z.; formal analysis, H.L. and X.H.; investigation, Y.M, Y.F. and X.H.; resources, S.H. and C.C.; data curation, S.H., Y.F., Y.M. and X.H.; writing—original draft preparation, S.H. and H.L.; writing—review and editing, S.H.; visualization, Y.F., and C.C.; supervision, S.H. and G.Z.; project administration, S.H. and G.Z.; funding acquisition, S.H. All authors have read and agreed to the published version of the manuscript.

Funding: This study was supported by the National Nature Science Foundation of China (No. 51965004).

Institutional Review Board Statement: Not applicable.

Informed Consent Statement: Not applicable.

Data Availability Statement: Not applicable.

Conflicts of Interest: The authors declare that the research was conducted in the absence of any commercial or financial relationships that could be construed as potential conflicts of interest.

References

1. Khashaba, U.A.; Abd-Elwahed, M.S.; Eltaher, M.A.; Najjar, I.; Ahmed, K.I. Thermo-mechanical and delamination properties in drilling gfrp composites by various drill angles. *Polymers* **2021**, *13*, 1884. [CrossRef]
2. Satheesh, C.; Sevvel, P.; Senthil, K.R. Experimental identification of optimized process parameters for fsw of az91c mg alloy using quadratic regression models. *J. Mech. Eng.* **2020**, *66*, 736–751. [CrossRef]
3. Ho-Cheng, H.; Dharan, C.K.H. Delamination During Drilling in Composite Laminates. *ASME J. Eng. Ind.* **1990**, *112*, 236–239. [CrossRef]
4. Hocheng, H.; Puw, H.Y. On drilling characteristics of fiber-reinforced thermoset and thermoplastics. *Int. J. Mach. Tools Manuf.* **1992**, *32*, 583–592. [CrossRef]
5. Won, M.S.; Dharan, C.K.H. Chisel Edge and Pilot Hole Effects in Drilling Composite Laminates. *ASME J. Manuf. Sci. Eng.* **2002**, *124*, 242–247. [CrossRef]
6. Turki, Y.; Habak, M.; Velasco, R.; Aboura, Z.; Khellil, K.; Vantomme, P. Experimental investigation of drilling damage and stitching effects on the mechanical behavior of carbon/epoxy composites. *Int. J. Mach. Tools Manuf. Des. Res. Appl.* **2014**, *87*, 61–72. [CrossRef]
7. Mohan, S.; Kulkarni, S.; Ramachandra, M. Delamination analysis in drilling process of glass fiber reinforced plastic (GFRP) composite materials. *J. Mater. Process. Technol.* **2007**, *186*, 265–271. [CrossRef]
8. Liu, L.; Qi, C.; Wu, F.; Xu, J.; Zhu, X. Experimental thrust forces and delamination analysis of GFRP laminates using candlestick drills. *Mater. Manuf. Process.* **2017**, *33*, 695–708. [CrossRef]

9. Zitoune, R.; Collombet, F.; Lachaud, F.; Piquet, R.; Pasquet, P. Experiment calculation comparison of the cutting conditions representative of the long fiber composite drilling phase. *Compos. Sci. Technol.* **2005**, *65*, 455–466. [CrossRef]
10. Palanikumar, K.; Davim, J.P. Assessment of some factors influencing tool wear on the machining of glass fibre-reinforced plastics by coated cemented carbide tools. *J. Mater. Process. Technol.* **2009**, *209*, 511–519. [CrossRef]
11. Gaugel, S.; Sripathy, P.; Haeger, A.; Meinhard, D.; Bernthaler, T.; Lissek, F.; Kaufeld, M.; Knoblauch, V.; Schneider, G. A comparative study on tool wear and laminate damage in drilling of carbon-fiber reinforced polymers (CFRP). *Compos. Struct.* **2016**, *155*, 173–183. [CrossRef]
12. Li, P.; Qiu, X.; Li, C.; Niu, Q.; Chen, A.; Ko, T.J. Hole exit damage and tool wear during the drilling of CFRP with a double-point angle drill. *J. Mech. Sci. Technol.* **2019**, *33*, 2363–2370. [CrossRef]
13. Liu, L.P.; Qi, C.L.; Wu, F.; Zhu, X. The effect of support on multi-hole drilling for glass fiber-reinforced plastic composite materials. *Int. J. Adv. Manuf. Technol.* **2017**, *93*, 953–965. [CrossRef]
14. Palanikumar, K.; Campos Rubio, J.; Abrao, A.M.; Esteves Correia, A.; Davim, J.P. Influence of Drill Point Angle in High Speed Drilling of Glass Fiber Reinforced Plastics. *J. Compos. Mater.* **2008**, *42*, 2585–2597. [CrossRef]
15. Mishra, R.; Malik, J.; Singh, I. Prediction of drilling-induced damage in unidirectional glass-fibre-reinforced plastic laminates using an artificial neural network. *J. Eng. Manuf.* **2010**, *224*, 733–738. [CrossRef]
16. Behera, R.R.; Ghadai, R.K.; Kalita, K.; Banerjee, S. Simul Banerjee. Simultaneous prediction of delamination and surface roughness in drilling GFRP composite using ANN. *Int. J. Plast. Technol.* **2016**, *20*, 424–450. [CrossRef]
17. Azmi, A.I.; Lin, R.J.T.; Bhattacharyya, D. Tool wear prediction models during end milling of glass fibre-reinforced polymer composites. *Int. J. Adv. Manuf. Technol.* **2013**, *67*, 701–718. [CrossRef]
18. Sathish Rao, U.; Rodrigues, L.L.R. Rodrigues. Comparative Analysis of Simulation of Different ANN Algorithms for Predicting Drill Flank Wear in the Machining of GFRP Composites. *Int. J. Appl. Eng. Res.* **2018**, *13*, 4102–4108.
19. Belaadi, A.; Boumaaza, M.; Alshahrani, H.; Bourchak, M. Effect of jute fiber length on drilling performance of biocomposites: Optimization comparison between RSM, ANN, and genetic algorithm. *Int. J. Adv. Manuf. Technol.* **2023**, *124*, 3579–3599. [CrossRef]
20. Prakash, S.; Suman, S. Neural network-based prediction for surface characteristics in CO2laser micro-milling of glass fiber reinforced plastic composite. *Neural Comput. Appl.* **2021**, *33*, 11517–11529. [CrossRef]
21. Cao, H.; Liu, L.; Wu, B.; Gao, Y.; Qu, D. Process optimization of high-speed dry milling UD-CF/PEEK laminates using GA-BP neural network. *Compos. Part B Eng.* **2021**, *221*, 109034. [CrossRef]
22. Kharwar, P.K.; Verma, R.K. Exploration of nature inspired Grey wolf algorithm and Grey theory in machining of multiwall carbon nanotube/polymer nanocomposites. *Eng. Comput.* **2022**, *38*, 1127–1148. [CrossRef]
23. Rubio, J.C.; Abrao, A.M.; Faria, P.E.; Correia, A.E.; Davim, J.P. Effects of high speed in the drilling of glass fibre reinforced plastic: Evaluation of the delamination factor. *Int. J. Mach. Tools Manuf.* **2008**, *48*, 715–720. [CrossRef]
24. Singaravel, B.; Radhika, M.; Asif, M.M.; Reddy, K.P. Analysis of hole quality errors in drilling of GFRP composite. *IOP Conf. Ser. Mater. Sci. Eng.* **2021**, *1057*, 012069. [CrossRef]
25. Sevvel, P.; Babu, S.; Kumar, R.S. Peak Temperature Correlation and Temperature Distribution during Joining of AZ80A Mg Alloy by FSW—A Numerical and Experimental Investigation. *J. Mech. Eng.* **2020**, *66*, 395–407. [CrossRef]
26. Erturk, A.T.; Vatansever, F.; Yarar, E.; Guven, E.A.; Sinmazcelik, T. Effects of cutting temperature and process optimization in drilling of GFRP composites. *J. Compos. Mater.* **2021**, *55*, 235–249. [CrossRef]
27. Upputuri, H.B.; Nimmagadda, V.S. Optimization of drilling process parameters used in machining of glass fiber reinforced epoxy composite. *Mater. Today Proc.* **2020**, *23*, 594–599. [CrossRef]
28. Dehghan, M.; Heidary, H. Parametric study on drilling of GFRP composite pipe produced by filament winding process in different backup condition. *Compos. Struct.* **2020**, *234*, 111661. [CrossRef]
29. Sevvel, P.; Satheesh, C.; Kumar, R.S. Generation of regression models and multi-response optimization of friction stir welding technique parameters during the fabrication of AZ80A Mg alloy joints. *Trans. Can. Soc. Mech. Eng.* **2020**, *44*, 311–324. [CrossRef]
30. Srinivasan, V.; Maheshkumar, K.V.; Karthikeyan, R.; Palanikumar, K. Application of Probablistic Neural Network for the Development of Wear Mechanism Map for Glass Fiber Reinforced Plastics. *J. Reinf. Plast. Compos.* **2007**, *26*, 1893–1906. [CrossRef]
31. Rao, U.S.; Lewlyn, L. Detecting Safety Zone Drill Process Parameters for Uncoated HSS Twist Drill in Machining GFRP Composites by Integrating Wear Rate and Wear Transition Mapping. *Indian J. Mater. Sci.* **2016**, *2016*, 9380583. [CrossRef]
32. Rumelhart, D.E.; Hinton, G.E.; Williams, R.J. Learning representations by back-propagating errors. *Nature* **1986**, *323*, 533–536. [CrossRef]
33. Rumelhart, D.E.; Hinton, G.E.; Williams, R.J. Learning Internal Representations by Error Propagation. *Read. Cogn. Sci.* **1988**, *323*, 399–421. [CrossRef]
34. Mirjalili, S.; Mirjalili, S.M.; Lewis, A.D. Grey Wolf Optimizer. *Adv. Eng. Soft* **2014**, *69*, 46–61. [CrossRef]

Disclaimer/Publisher's Note: The statements, opinions and data contained in all publications are solely those of the individual author(s) and contributor(s) and not of MDPI and/or the editor(s). MDPI and/or the editor(s) disclaim responsibility for any injury to people or property resulting from any ideas, methods, instructions or products referred to in the content.